LETTER

Corrected: Author Correction

https://doi.org/10.1038/s41586-018-0158-3

A global slowdown of tropical-cyclone translation speed

James P. Kossin[1]*

As the Earth's atmosphere warms, the atmospheric circulation changes. These changes vary by region and time of year, but there is evidence that anthropogenic warming causes a general weakening of summertime tropical circulation[1–8]. Because tropical cyclones are carried along within their ambient environmental wind, there is a plausible a priori expectation that the translation speed of tropical cyclones has slowed with warming. In addition to circulation changes, anthropogenic warming causes increases in atmospheric water-vapour capacity, which are generally expected to increase precipitation rates[9]. Rain rates near the centres of tropical cyclones are also expected to increase with increasing global temperatures[10–12]. The amount of tropical-cyclone-related rainfall that any given local area will experience is proportional to the rain rates and inversely proportional to the translation speeds of tropical cyclones. Here I show that tropical-cyclone translation speed has decreased globally by 10 per cent over the period 1949–2016, which is very likely to have compounded, and possibly dominated, any increases in local rainfall totals that may have occurred as a result of increased tropical-cyclone rain rates. The magnitude of the slowdown varies substantially by region and by latitude, but is generally consistent with expected changes in atmospheric circulation forced by anthropogenic emissions. Of particular importance is the slowdown of 21 per cent and 16 per cent over land areas affected by western North Pacific and North Atlantic tropical cyclones, respectively, and the slowdown of 22 per cent over land areas in the Australian region. The unprecedented rainfall totals associated with the 'stall' of Hurricane Harvey[13–15] over Texas in 2017 provide a notable example of the relationship between regional rainfall amounts and tropical-cyclone translation speed. Any systematic past or future change in the translation speed of tropical cyclones, particularly over land, is therefore highly relevant when considering potential changes in local rainfall totals.

There is complex interaction between the internal and external factors that control tropical-cyclone intensity[16,17], which is generally described in terms of cyclonic rotation speed. In addition to a rotation speed, tropical cyclones also have a translation speed that is controlled largely by the environmental steering winds in which they are embedded. The maximum tropical-cyclone intensity experienced at ground level is to the right (left) of the translation vector in the Northern (Southern) Hemisphere, where the rotation and translation speeds are summed. Consequently, a slowing of the tropical-cyclone translation speed would reduce the maximum ground-relative intensity in both hemispheres. The ratio of translation to rotation speed can be close to or greater than unity in weaker tropical cyclones, particularly outside of the tropics where the ambient steering winds can be strong. But this ratio is generally small for the more societally relevant, intense tropical cyclones, particularly those translating within the comparatively weak tropical trade winds; in this case, a slowing of translation speed would have a proportionally small effect on the ground-relative maximum intensity. Alternatively, a slowing of translation speed could have a profound effect on the amount of local, tropical-cyclone-related rainfall, which is proportional to the rate of rain produced in a tropical cyclone and inversely proportional to its translation speed; that is, a proportional unit of decrease in translation speed would have about the same effect on local rainfall totals as the same proportional unit of increase in rain rate.

Anthropogenic warming, both past and projected, is expected to affect the strength and patterns of global atmospheric circulation[1–8]. Tropical cyclones are generally carried along within these circulation patterns so their past translation speeds may be indicative of past circulation changes. In particular, warming is linked to a weakening of tropical summertime circulation and there is a plausible a priori expectation that tropical-cyclone translation speed may be decreasing. In addition to changing circulation, anthropogenic warming is expected to increase lower-tropospheric water-vapour capacity by about 7% per degree (Celsius) of warming, as per the Clausius–Clapeyron relationship[2]. Expectations of increased mean precipitation under global warming are well documented, but not as straightforward to quantify[9,18]. Increases in global precipitation are constrained by the atmospheric energy budget to about 1%–2% per degree of warming[19,20]; those in regional precipitation are further controlled by variability in moisture convergence driven by variability in regional circulation. Precipitation extremes can vary more broadly and are less constrained by energy considerations than is global precipitation[21–24].

Numerical simulations of tropical-cyclone rain rates are fairly consistent in projecting increases in a warming world[10–12]. Tropical cyclones are very effective at converging moisture, and rain-rate increases tend to be largest near their centres, where the convergence is greatest; further from their centres, simulated rain-rate increases tend to be smaller. Close to the centre of a tropical cyclone, rain-rate increases can exceed the 7% per degree of warming indicated by the Clausius–Clapeyron scaling. In recent global simulations, the maximum increase in rain rate was estimated to be about 10% per degree of warming[25]. Therefore, anthropogenic warming is expected to increase the rain rates and decrease the translation speeds of tropical cyclones. Because the amount of local tropical-cyclone-related rainfall depends on both rain rate and translation speed (with a decrease in translation speed having about the same local effect, proportionally, as an increase in rain rate, as noted above), each of these two independent effects of anthropogenic warming is expected to increase local rainfall. The increase in local rainfall caused by a 10% global increase in the tropical-cyclone rain rate per degree of warming, as predicted in numerical simulations[25], would be doubled by a concurrent slowdown in tropical-cyclone translation speed of as little as 10%. In addition, increases in tropical-cyclone rain rate due to warming become smaller further from the tropical-cyclone centre, such that rain-band rain rates increase by only a fraction of the simulated increase in rain-rates under the eyewall[10–12,25]. There is no such relationship for translation speed, so a slowdown in translation speed will increase local rainfall amounts by the same percentage at all distances from the tropical-cyclone centre. This further strengthens the potential for the effect of past and projected changes in translation speed to dominate that of changes in rain rate.

[1]NOAA National Centers for Environmental Information, Center for Weather and Climate, Madison, WI, USA. e-mail: james.kossin@noaa.gov

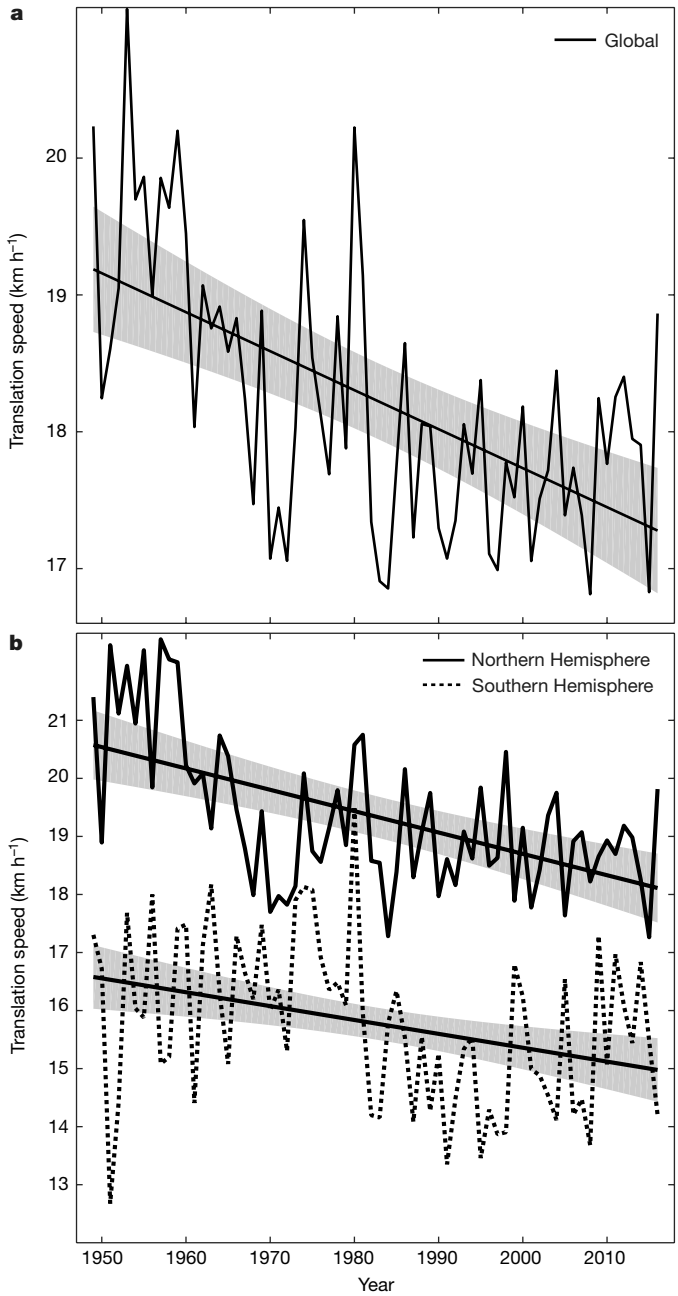

Fig. 1 | Global and hemispheric time series of annual-mean tropical-cyclone translation speed and their linear trends. a, **b**, The period of the time series is 1949–2016. Gray shading indicates the two-sided 95% confidence bounds of the trends, which have been adjusted for autocorrelation as needed (see Methods). Time series are shown for the global data (**a**) and for the data separated by Northern and Southern hemispheres (**b**). The trends for the global and Northern Hemisphere data have confidence levels of about 100% (based on *P* values; see Extended Data Table 1). The trend in the Southern Hemisphere is significant at about the 99% two-sided confidence level.

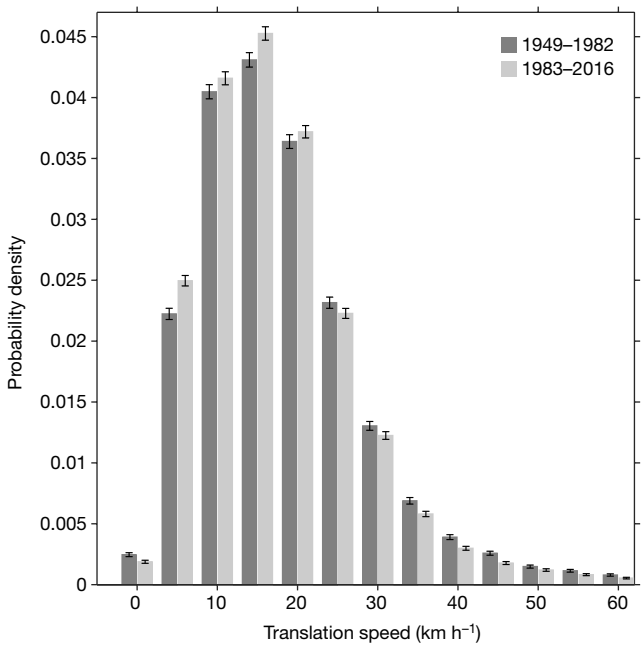

Fig. 2 | Change in the global distribution of tropical-cyclone translation speed. The changes are shown between the first and second halves of the period 1949–2016. Error bars show two-sided 95% confidence intervals based on bootstrap sampling (see Methods). There are significantly higher probabilities of translation speeds of less than 20 km h^{-1} in the later period and significantly higher probabilities of translations speeds of greater than 20 km h^{-1} in the earlier period.

Time series of annual-mean global and hemispheric translation speed are shown in Fig. 1, based on global tropical-cyclone 'best-track' data (see Methods). A highly significant global slowdown of tropical-cyclone translation speed is evident, of −10% over the 68-yr period 1949–2016 (Extended Data Table 1). During this period, global-mean surface temperature has increased by about 0.5 °C[9]. The global distribution of translation speed exhibits a clear shift towards slower speeds in the second half of the 68-yr period, and the differences are highly significant throughout most of the distribution (Fig. 2). This slowing is found in both the Northern and Southern Hemispheres (Fig. 1), but is stronger and more significant in the Northern Hemisphere, where the annual number of tropical cyclones is generally greater. The times series for the Southern Hemisphere exhibits a change-point around 1980, but the reason for this is not clear. Before 1980, analyses of tropical cyclones depended largely on polar orbiting satellites to provide estimates of tropical-cyclone centre position; after 1980, geostationary satellites were also available. Such a change in the availability of satellite information is expected to introduce heterogeneity into estimates of tropical-cyclone intensity[26], but estimates of tropical-cyclone position should be comparatively insensitive to such changes. In addition, estimates of translation speed should be comparatively insensitive to less-than-perfect estimates of tropical-cyclone position along the tropical-cyclone track because the speed is calculated between each pair of positions, and position errors along the track should mostly cancel each other when the speeds are averaged along the track.

The trends in tropical-cyclone translation speed and their signal-to-noise ratios vary considerably when the data are parsed by region, but slowing is found in every basin except the northern Indian Ocean (Extended Data Fig. 1, Extended Data Table 1). Significant slowings of −16% in the western North Pacific Ocean and of −14% in the region around Australia (Southern Hemisphere, east of 100° E) are observed. When the data are constrained within global latitude belts (Extended Data Fig. 2, Extended Data Table 1), significant slowing is observed at latitudes between 15° and 25° N and between 0° and 30° S. Slowing trends near the equator tend to be smaller and not significant, whereas there is a substantial (but insignificant) increasing trend in translation speed at higher latitudes in the Southern Hemisphere.

When only that data that correspond to tropical cyclones over water are considered, which amounts to about 90% of the global best-track data, the trend statistics are indistinguishable from the global slowing trends (Extended Data Table 1). The 10% of the global data that correspond to tropical cyclones over land, where local rainfall effects become more societally relevant, exhibits a weak and insignificant increasing trend. However, changes in tropical-cyclone translation speed over land vary substantially by region (Fig. 3, Extended Data Table 1). There is a substantial and significant slowing trend over land areas affected

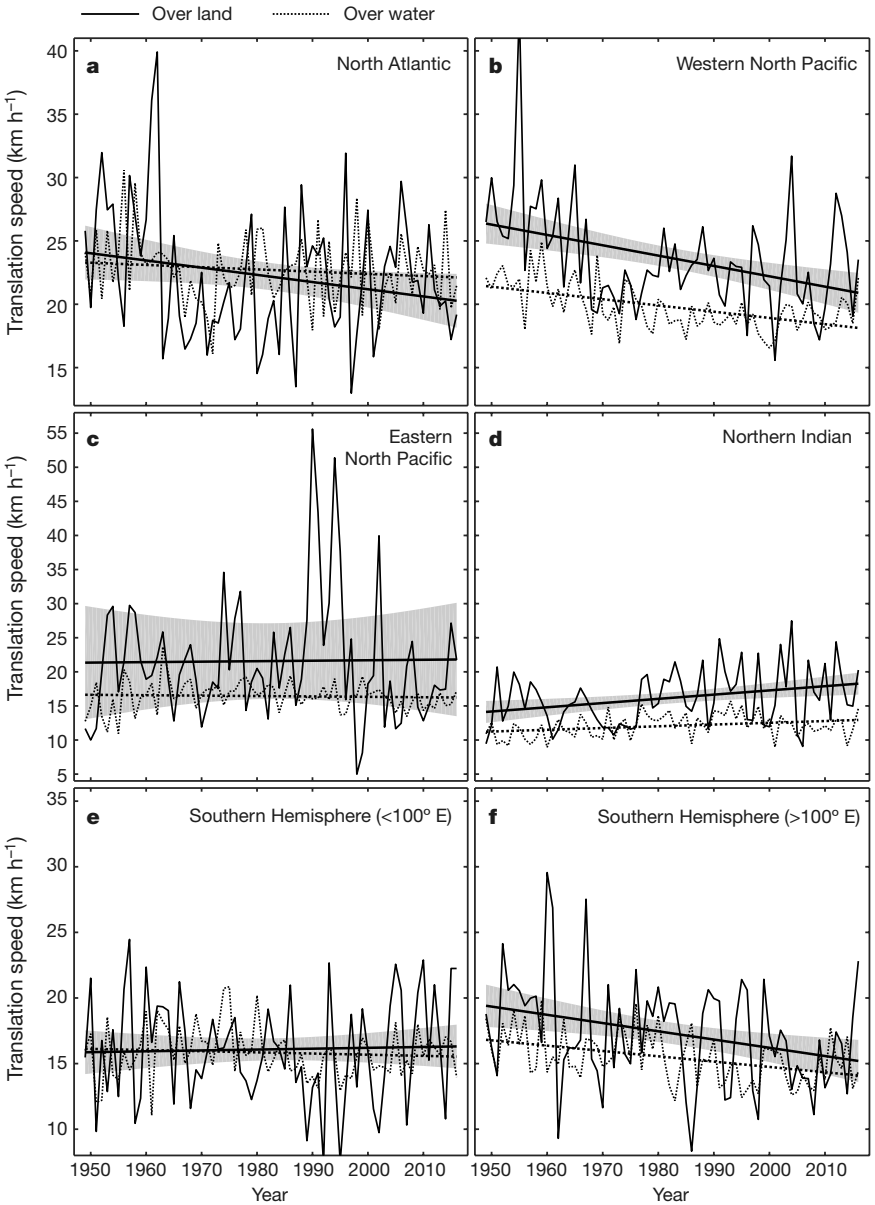

Fig. 3 | Time series of annual-mean tropical-cyclone translation speed and their linear trends over land and water. a–f, Time series are shown for the individual ocean basins, over land (solid lines) and water (dotted lines). Grey shading indicates the two-sided 95% confidence bounds of the trends over land, corrected for autocorrelation as needed. The regions are the North Atlantic (**a**), western North Pacific (**b**), eastern North Pacific (**c**) and northern Indian (**d**) basins, and the regions west (**e**) and east (**f**) of 100° E in the Southern Hemisphere. The regions over land that are affected in each region are shown in Extended Data Fig. 3.

by western North Pacific tropical cyclones (21% reduction) and by tropical cyclones in the Australian region (22% reduction), and a slowing trend of 16% over land areas affected by North Atlantic storms (significant at 90%). These trends have almost certainly increased local rainfall totals in these regions, which are more difficult to measure directly. Contrarily, the tropical-cyclone translation speeds over land areas affected by eastern North Pacific and northern Indian tropical cyclones, and of tropical cyclones that have affected Madagascar and the east coast of Africa, all exhibit positive trends (significant in the northern Indian Ocean). Note that several of the time series shown here exhibit outliers that suggest non-normality of the residuals from the trend lines; a discussion and analysis of the robustness of the trends presented here is provided in Methods.

None of the analyses presented here has any dependence on tropical-cyclone intensity; in some cases, the translation speeds were calculated in the absence of any concurrent intensity estimates in the best-track data (cases where location but not intensity information is available). This allows much greater confidence in the homogeneity of the historical best-track data, but does not allow for intensity-based stratifications of the data. This is a caveat of these analyses because tropical-cyclone rain rates have been shown to be a function of their intensity, with greater rates linked to stronger tropical cyclones[27]. In this case, there is a possibility for offsetting the effects of tropical-cyclone slowdown if the trends in translation speed are dominated by weaker systems and for compounding these effects if the trends are dominated by stronger systems. This is left as an open question.

The analyses presented here do not constitute a detection and attribution study because there are likely to be many factors, natural and anthropogenic, that control tropical-cyclone translation speed. For example, the best-track data exhibit a global 10% reduction in translation speed during a period in which global-mean surface temperatures increased by about 0.5 °C; however, this finding does not provide a true measure of the climate sensitivity of these related phenomena. To determine the true sensitivity (that is, the expected change in translation

speed as a function of anthropogenic forcing), further analyses and numerical simulations are required.

In addition to the global slowing of tropical-cyclone translation speed identified here, there is evidence that tropical cyclones have migrated poleward in several regions[28]. Of particular relevance here, the rate of migration in the western North Pacific was found to be large, which has had a substantial effect on regional tropical-cyclone-related hazard exposure[29]. When this finding is considered in tandem with the substantial slowdown of translation speed over land in this region (21% since 1949), the potential for increased hazard exposure becomes greater still, particularly to fresh-water flooding hazards, which can pose an especially large mortality risk[30]. Further compounding these changes in regional exposure, the projected increases in tropical-cyclone rain rate in the western North Pacific for the late twenty-first century are about twice the projected global-mean increase[25]. These recently identified trends in tropical-cyclone track behaviour emphasize that tropical-cyclone frequency and intensity should not be the only metrics considered when establishing connections between climate variability and change and the risks associated with tropical cyclones, both past and future. These trends further support the idea that the behaviours of tropical cyclones are being altered in societally relevant ways by anthropogenic factors. Continued research into the connections between tropical cyclones and climate is essential to understanding and predicting the changes in risk that are occurring on a global scale.

The analyses presented here demonstrate changes in the behaviour of translation speed, but local rainfall totals are also affected by translation direction. For example, a tropical cyclone that follows a looping track over some region could be translating quickly along the loop, but the rainfall totals in the region would still be large owing to the spatially confined track. In 2017, Hurricane Harvey not only translated slowly over Texas but also reversed direction and thus affected the same region over a particularly long duration. There is currently no formal definition of what constitutes a 'stalled track', although this term has been used to describe the track of Hurricane Harvey. Future studies that focus on tropical cyclones that remain geographically constrained for extended durations are warranted.

Online content

Any Methods, including any statements of data availability and Nature Research reporting summaries, along with any additional references and Source Data files, are available in the online version of the paper at https://doi.org/10.1038/s41586-018-0158-3.

Received: 22 February 2018; Accepted: 18 April 2018;
Published online: 06 June 2018

1. Mann, M. E. et al. Influence of anthropogenic climate change on planetary wave resonance and extreme weather events. *Sci. Rep.* **7**, 19831 (2017).
2. Held, I. M. & Soden, B. J. Robust responses of the hydrological cycle to global warming. *J. Clim.* **19**, 5686–5699 (2006).
3. He, J. & Soden, B. J. Anthropogenic weakening of the tropical circulation: the relative roles of direct CO_2 forcing and sea surface temperature change. *J. Clim.* **28**, 8728–8742 (2015).
4. Coumou, D., Lehmann, J. & Beckmann, J. The weakening summer circulation in the Northern Hemisphere mid-latitudes. *Science* **348**, 324–327 (2015).
5. Vecchi, G. A. & Soden, B. J. Global warming and the weakening of the tropical circulation. *J. Clim.* **20**, 4316–4340 (2007).
6. Vecchi, G. A. et al. Weakening of tropical Pacific atmospheric circulation due to anthropogenic forcing. *Nature* **441**, 73–76 (2006).
7. Grise, K. M. & Polvani, L. M. Understanding the timescales of the tropospheric circulation response to abrupt CO_2 forcing in the Southern Hemisphere: seasonality and the role of the stratosphere. *J. Clim.* **30**, 8497–8515 (2017).
8. He, C., Wu, B., Zou, L. & Zhou, T. Responses of the summertime Subtropical Anticyclones to global warming. *J. Clim.* **30**, 6465–6479 (2017).
9. Hartmann, D. L. et al. in *Climate Change 2013: The Physical Science Basis. Contribution of Working Group I to the Fifth Assessment Report of the Intergovernmental Panel on Climate Change* (eds Stocker, T. F. et al.) 159–254 (Cambridge Univ. Press, Cambridge, 2013).
10. Christensen, J. H. et al. in *Climate Change 2013: The Physical Science Basis. Contribution of Working Group I to the Fifth Assessment Report of the Intergovernmental Panel on Climate Change* (eds Stocker, T. F. et al.) 1217–1308 (Cambridge Univ. Press, Cambridge, 2013).
11. Kossin, J. P. et al. in *Climate Science Special Report: Fourth National Climate Assessment* Vol. I (eds Wuebbles, D. J. et al.) 257–276 (US Global Change Research Program, Washington DC, 2017).
12. Walsh, K. J. E. et al. Tropical cyclones and climate change. *Wiley Interdiscip. Rev. Clim. Change* **7**, 65–89 (2016).
13. Emanuel, K. A. Assessing the present and future probability of Hurricane Harvey's rainfall. *Proc. Natl Acad. Sci. USA* **114**, 12681–12684 (2017).
14. Risser, M. D., & Wehner, M. F. Attributable human-induced changes in the likelihood and magnitude of the observed extreme precipitation during Hurricane Harvey. *Geophys. Res. Lett.* **44**, 12457–12464 (2017).
15. van Oldenborgh, G. J. et al. Attribution of extreme rainfall from Hurricane Harvey, August 2017. *Environ. Res. Lett.* **12**, 124009 (2017); corrigendum **13**, 019501 (2018).
16. DeMaria, M., Mainelli, M., Shay, L. K., Knaff, J. A. & Kaplan, J. Further improvement to the Statistical Hurricane Intensity Prediction Scheme (SHIPS). *Weather Forecast.* **20**, 531–543 (2005).
17. Kossin, J. P. & Sitkowski, M. Predicting hurricane intensity and structure changes associated with eyewall replacement cycles. *Weather Forecast.* **27**, 484–488 (2012).
18. Hegerl, G. E. et al. Challenges in quantifying changes in the global water cycle. *Bull. Am. Meteorol. Soc.* **96**, 1097–1115 (2015).
19. Allen, M. R. & Ingram, W. J. Constraints on future changes in climate and the hydrologic cycle. *Nature* **419**, 224–232 (2002).
20. Pendergrass, A. G. & Hartmann, D. L. The atmospheric energy constraint on global-mean precipitation change. *J. Clim.* **27**, 757–768 (2014).
21. Allan, R. F. & Soden, B. J. Atmospheric warming and the amplification of precipitation extremes. *Science* **321**, 1481–1484 (2008).
22. Kitoh, A. & Endo, H. Changes in precipitation extremes projected by a 20-km mesh global atmospheric model. *Weather Clim. Extrem.* **11**, 41–52 (2016).
23. Kharin, V. V., Zwiers, F. W., Zhang, X. & Wehner, M. Changes in the temperature and precipitation extremes in the CMIP5 ensemble. *Clim. Change* **119**, 345–357 (2013).
24. Prein, A. F. et al. The future intensification of hourly precipitation extremes. *Nat. Clim. Chang.* **7**, 48–52 (2017).
25. Knutson, T. R. et al. Global projections of intense tropical cyclone activity for the late twenty-first century from dynamical downscaling of CMIP5/RCP4.5 scenarios. *J. Clim.* **28**, 7203–7224 (2015).
26. Kossin, J. P., Olander, T. L. & Knapp, K. R. Trend analysis with a new global record of tropical cyclone intensity. *J. Clim.* **26**, 9960–9976 (2013).
27. Lonfat, M., Marks, F. D. & Chen, S. Precipitation distribution in tropical cyclones using the Tropical Rainfall Measuring Mission (TRMM) microwave imager: a global perspective. *Mon. Weath. Rev.* **132**, 1645–1660 (2004).
28. Kossin, J. P., Emanuel, K. A. & Vecchi, G. A. The poleward migration of the location of tropical cyclone maximum intensity. *Nature* **509**, 349–352 (2014).
29. Kossin, J. P., Emanuel, K. A. & Camargo, S. J. Past and projected changes in western North Pacific tropical cyclone exposure. *J. Clim.* **29**, 5725–5739 (2016).
30. Rappaport, E. N. Loss of life in the United States associated with recent Atlantic tropical cyclones. *Bull. Am. Meteorol. Soc.* **81**, 2065–2073 (2000).

Acknowledgements This work was supported by NOAA's National Centers for Environmental Information.

Reviewer information *Nature* thanks M. Mann and C. Patricola for their contribution to the peer review of this work.

Competing interests The author declares no competing interests.

Additional information
Extended data is available for this paper at https://doi.org/10.1038/s41586-018-0158-3.
Reprints and permissions information is available at http://www.nature.com/reprints.
Correspondence and requests for materials should be addressed to J.P.K.
Publisher's note: Springer Nature remains neutral with regard to jurisdictional claims in published maps and institutional affiliations.

METHODS

Best-track data are taken from IBTrACS[31] (see Methods section 'Data availability'). On the basis of comparisons of IBTrACS data sources[32], data from the US National Hurricane Center (NHC) and Joint Typhoon Warning Center (JTWC) were combined to provide global coverage. NHC data cover the North Atlantic and eastern North Pacific oceans. JTWC data cover the western North Pacific and northern Indian oceans and the Southern Hemisphere, which includes the southern Indian and South Pacific oceans. 100° E was used to separate tropical cyclones that affect the Australia region from those that affect Madagascar and the east coast of Africa. The analyses presented here are not highly sensitive to this choice. The period 1949–2016 was chosen on the basis of uniform availability of data from each region.

Time series are based on annual-mean translation speeds. Translation speed is calculated using neighbouring positions along each tropical-cyclone track (these are provided in six-hourly intervals throughout the lifetime of each tropical cyclone). Distances between locations are calculated along a great circle arc. Trends are estimated by linear regression. The *P* values of the regression are based on the full degrees of freedom in the 68-year time series. Because some of the time series exhibit autoregressive (AR(1)) persistence, as determined from a Durbin–Watson test, confidence intervals are provided with degrees of freedom adjusted when needed. Statistical significance is based on the two-sided 95% confidence intervals (not the *P* values).

The percentage change is calculated by dividing the difference between the last and first points of the best-fit trend line by the first point. Over-land positions are determined using a high-resolution global topography map (see Methods section 'Data availability'). If either one or both of the two locations used to calculate the translation speed are over land, then the speed is considered to be an over-land speed. The two-sided 95% confidence bounds on the probability-density histogram (Fig. 2) are constructed by repeated random sampling with replacement within each of the two time periods. The error bars show $\pm 2\sigma$ from the mean in each histogram bin.

The final post-season-reanalysed NHC and JTWC data for 2017 were not yet available at the time of writing this manuscript, but it is interesting to identify Hurricane Harvey's effect on the 2017-mean tropical-cyclone translation speed over land that is affected by Atlantic hurricanes. Using the 'operational best-track' data from the Automated Tropical Cyclone Forecasting System (ATCF)[33], the 2017-mean over-land Atlantic translation speed is 17.9 km h^{-1}, which is at the slowest 20th percentile of over-land translation speeds for the period since 1949. Adding this point to the annual time series slightly increases the magnitude of the slowing trend and decreases the *P* value of the regression to 0.0200 (from 0.0275).

To test the robustness of the trends shown here, particularly to outliers, which are evident in several of the time series shown and could indicate a non-Gaussian distribution of the regression residuals, all trends were recalculated using the L^1 norm in place of the L^2 (ordinary least-squares) norm (Extended Data Table 2). A few of the trends are slightly affected by this choice, but none of the significant trends from the L2 regressions becomes insignificant. Still, the trend statistics presented here should be interpreted with the understanding that the distribution of the regression residuals may deviate from normal (Extended Data Figs. 4, 5), particularly when the global data are parsed to smaller subregions. Caution in interpretation is particularly important for slowing trends in over-land translation speed in regions that exhibit clear positive outliers in the early part of the time series. On the other hand, some additional confidence is found in the general agreement in the sign of the trend between the basins as a whole and the subsampled over-land regions. Similarly, the global trend (Fig. 1a) is not very sensitive to the removal of individual points or to small changes in the start and end points of the time series, but these sensitivities increase, as expected, when the global data are subsampled down to progressively finer regional scales.

The poleward migration of tropical cyclones discussed above could be related to the slowdown of translation speed via tropical-cyclone 'beta drift'[34]. In particular, a poleward migration would reduce beta drift, which, all other things being equal, would reduce the translation speed. In addition, a decrease in mean tropical-cyclone intensity would reduce the translation speed through beta drift; however, no such decrease has been observed in the period considered here and there is some evidence that mean tropical-cyclone intensity has increased since the early 1980s[26,35]. The potential relationships, based on beta-drift arguments, between the translation speed, poleward migration and intensity of tropical cyclones warrants further study.

The colour choices in Extended Data Figs. 2 and 3 follow a specification designed to mitigate colour blindness[36].

No statistical methods were used to predetermine sample size.

Data availability. The tropical-cyclone data analysed during this study were taken from the International Best Track Archive for Climate Stewardship (IBTrACS; https://www.ncdc.noaa.gov/ibtracs/, file 'Allstorms.ibtracs_all.v03r10.nc'). The over-land tropical-cyclone positions were determined from the 2-Minute Gridded Global Relief Data (ETOPO2v2; https://www.ngdc.noaa.gov/mgg/global/etopo2.html). These data are also available from the corresponding author on request.

Code availability. All codes used to read, analyse and plot the data are available from the corresponding author on request.

31. Knapp, K. R., Kruk, M. C., Levinson, D. H., Diamond, H. J. & Neumann, C. J. The International Best Track Archive for Climate Stewardship (IBTrACS). *Bull. Am. Meteorol. Soc.* **91**, 363–376 (2010).
32. Schreck, C. J. III, Knapp, K. R. & Kossin, J. P. The impact of best track discrepancies on global tropical cyclone climatologies using IBTrACS. *Mon. Weath. Rev.* **142**, 3881–3899 (2014).
33. Sampson, C. R. & Schrader, A. J. The automated tropical cyclone forecasting system (version 3.2)". *Bull. Am. Meteorol. Soc.* **81**, 1231–1240 (2000).
34. Smith, R. B. A hurricane beta-drift law. *J. Atmos. Sci.* **50**, 3213–3215 (1993).
35. Elsner, J. B., Kossin, J. P. & Jagger, T. H. The increasing intensity of the strongest tropical cyclones. *Nature* **455**, 92–95 (2008).
36. Wong, B. Points of view: Color blindness. *Nat. Methods* **8**, 441 (2011).

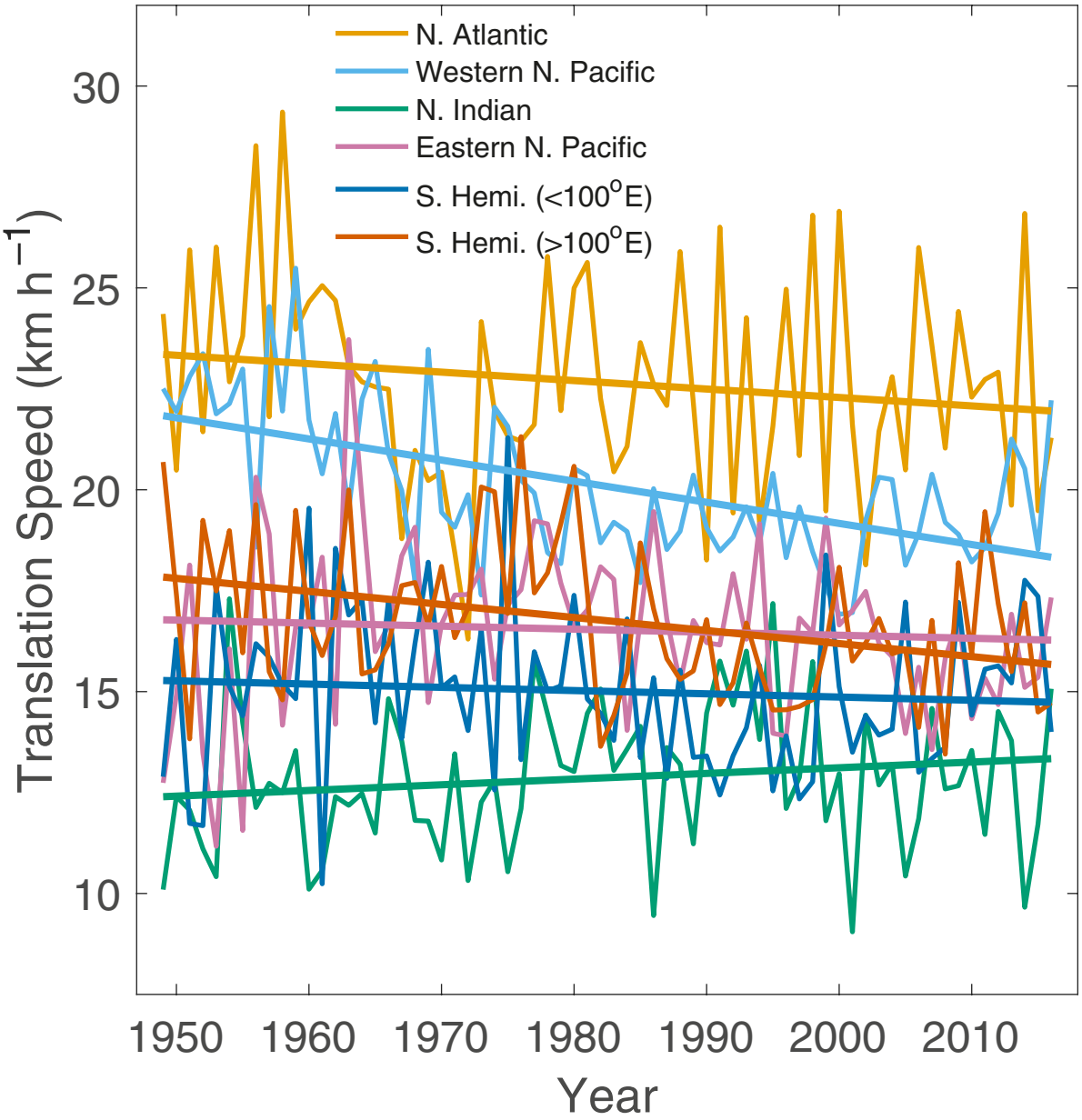

Extended Data Fig. 1 | Time series of annual-mean tropical-cyclone translation speed and their linear trends in varying ocean basins. Time series are shown for the individual ocean basins: North Atlantic, western North Pacific, northern Indian, eastern North Pacific, and the regions west and east of 100° E in the Southern Hemisphere.

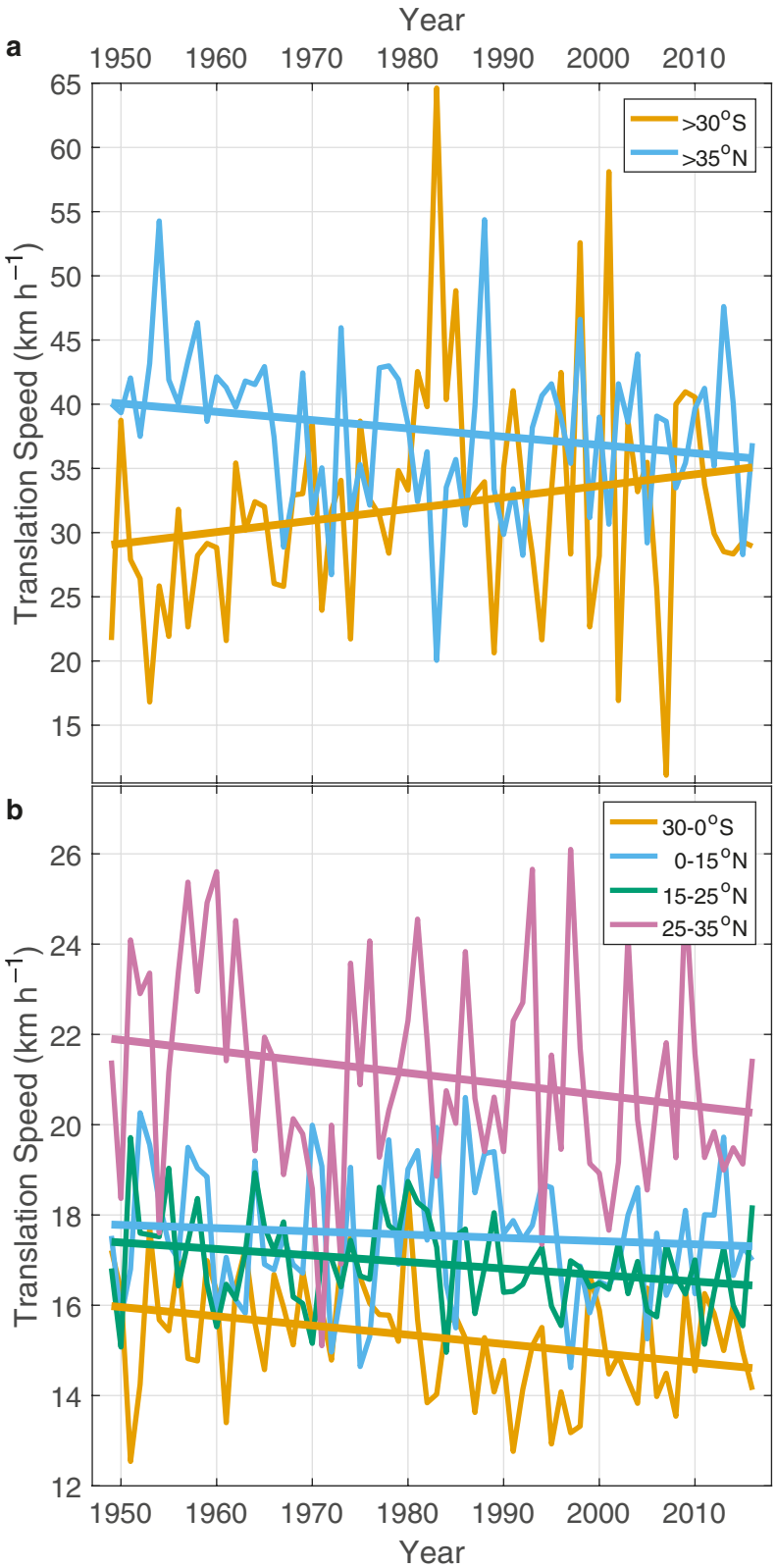

Extended Data Fig. 2 | Time series of annual-mean tropical-cyclone translation speed and their linear trends in varying latitude belts. **a**, **b**, Time series are shown for global latitude belts southward (poleward) of 30° S and northward (poleward) of 35° N (**a**), and in the belts 30°–0° S, 0°–15° N, 15°–25° N and 25–35° N (**b**). The broader latitude belts defined in the less-active Southern Hemisphere were needed to have a large enough sample of tropical cyclones in each to perform the analyses. The analyses shown here are fairly robust to the choice of latitude-belt bounds.

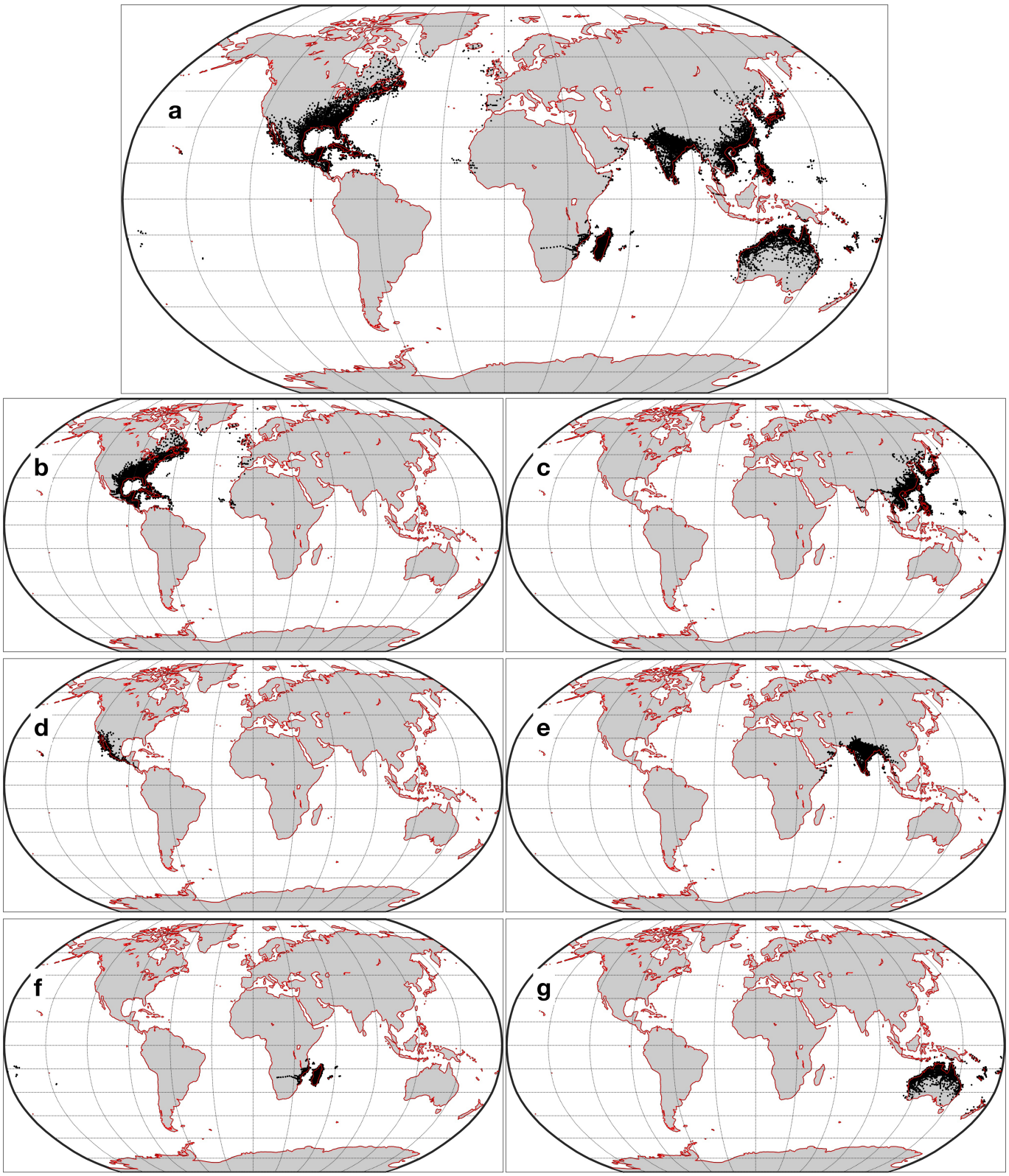

Extended Data Fig. 3 | Best-track tropical-cyclone centre locations for tropical-cyclone translation speeds over land. Locations (black dots) are shown for the regions considered in Fig. 3 and Extended Data Table 1. **a**–**g**, Over-land positions are shown for land areas affected by tropical cyclones globally (**a**), in the North Atlantic (**b**), western North Pacific (**c**), eastern North Pacific (**d**) and northern Indian (**e**) basins, and in the regions west (**f**) and east (**g**) of 100° E in the Southern Hemisphere.

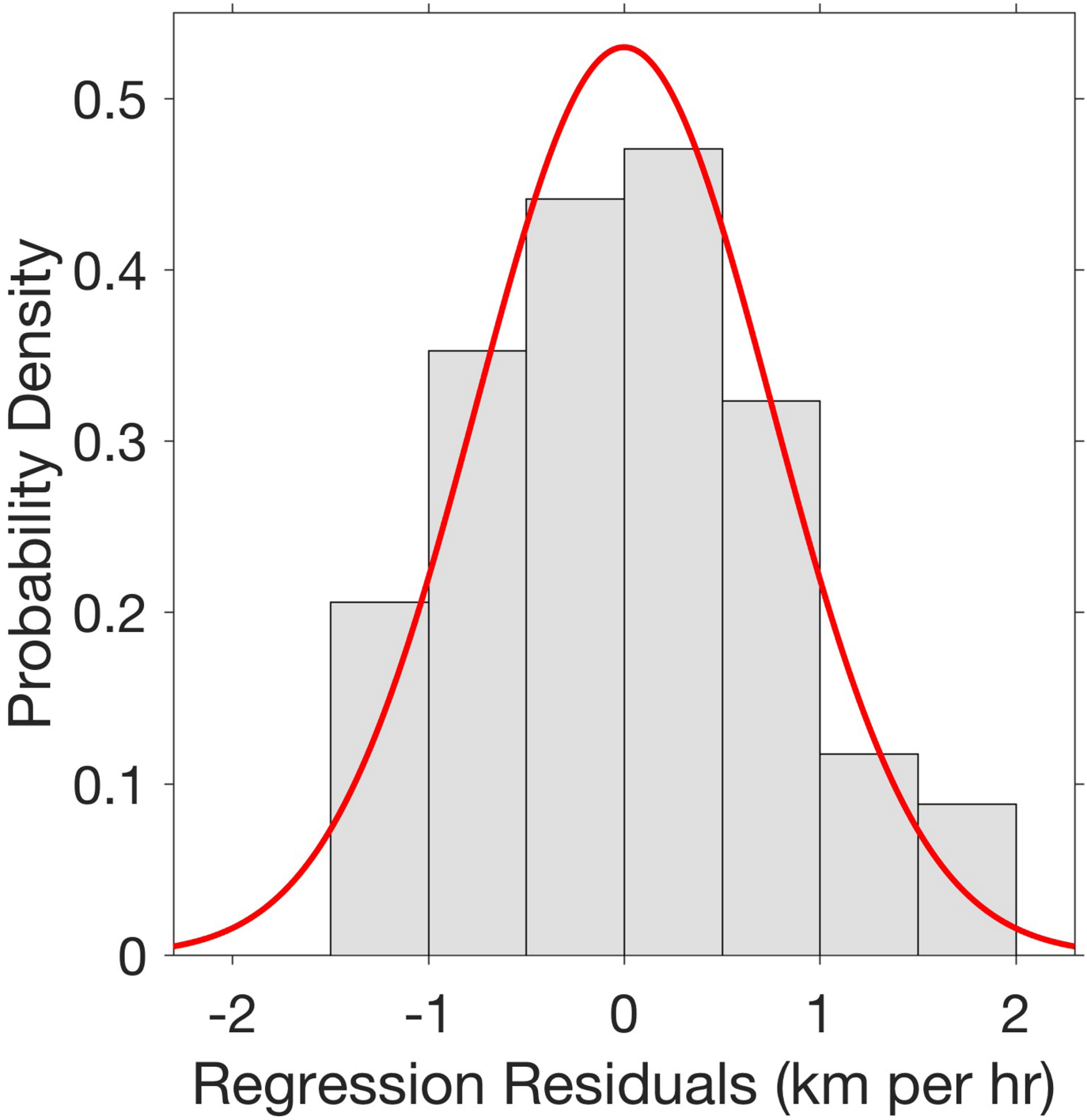

Extended Data Fig. 4 | Distribution of the residuals from the ordinary least-squares regression. The histogram shows the distribution of residuals from the trend for the time series of annual-mean global tropical-cyclone translation speed shown in Fig. 1a. The normal distribution is shown in red.

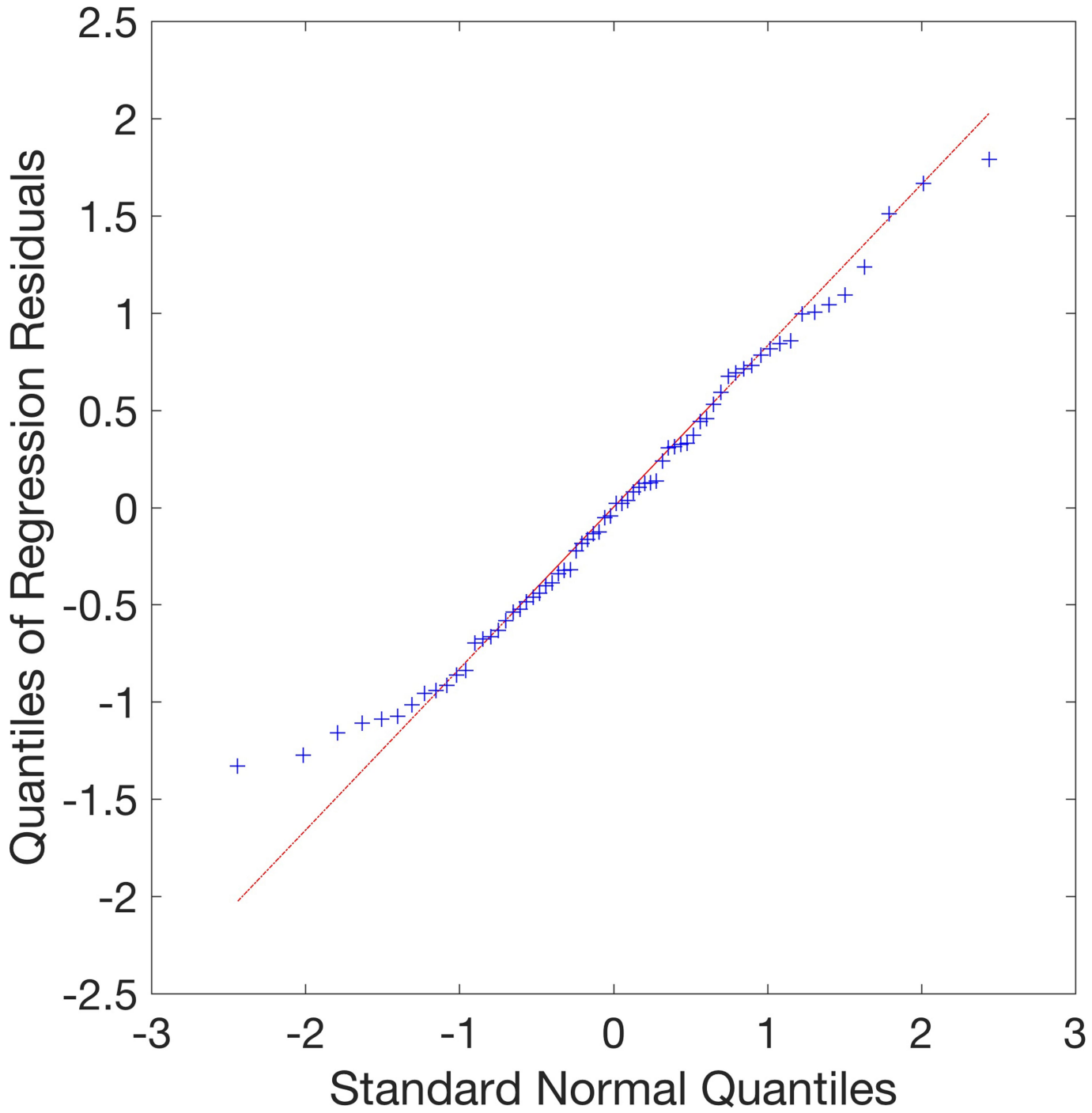

Extended Data Fig. 5 | Quantile–quantile plot for the residuals of the global ordinary least-squares regression. The left tail of the distribution is thinner than the normal distribution, which suggests that the likelihood of an extremely slow translation speed is less than would be found in a normally distributed sample.

Extended Data Table 1 | Trends in tropical-cyclone translation speed and their statistics

	Trend ($km\ h^{-1}\ yr^{-1}$)	Change (%)	p-value (uncorrected)	95% confidence interval of the trend
Global	**–0.03**	**–10**	$<10^{-7}$	[–0.04, –0.02]*
N. Hemisphere	**–0.04**	**–12**	$<10^{-7}$	[–0.05, –0.02]
S. Hemisphere	**–0.02**	**–10**	0.006	[–0.04, –0.008]*
N. Atlantic	–0.02	–6	0.20	[–0.05, 0.011]
Western N. Pacific	**–0.05**	**–16**	$<10^{-7}$	[–0.07, –0.03]
Eastern N. Pacific	–0.01	–3	0.57	[–0.03, 0.02]
N. Indian	+0.01	+8	0.21	[–0.01, 0.04]
S. Hemi. (<100°E)	–0.01	–4	0.49	[–0.03, 0.02]
S. Hemi. (≥100°E)	**–0.04**	**–14**	$<10^{-3}$	[–0.06, –0.02]
>35°N	–0.06	–11	0.09	[–0.14, 0.008]
25–35°N	–0.02	–7	0.10	[–0.05, 0.004]
15–25°N	**–0.01**	**–6**	0.02	[–0.03, –0.003]
0–15°N	–0.01	–3	0.43	[–0.02, 0.01]
0–30°S	**–0.02**	**–9**	0.01	[–0.04, –0.006]
> 30°S	+0.09	+21	0.11	[–0.02, 0.20]
Global (water)	**–0.03**	**–11**	$<10^{-7}$	[–0.04, –0.02]
Global (land)	0.00	+2	0.76	[–0.04, 0.05]*
N. Atlantic (land)	–0.06	–16	0.08	[–0.12, 0.006]
W. N. Pacific (land)	**–0.08**	**–21**	0.001	[–0.13, –0.03]
E. N. Pacific (land)	+0.01	+2	0.90	[–0.17, 0.18]*
N. Indian (land)	**+0.06**	**+29**	0.01	[–0.01, 0.11]
S. Hemi. (<100°E, land) Madagascar	+0.01	+3	0.80	[–0.04, 0.06]
S. Hemi. (≥100°E, land) Australia	**–0.06**	**–22**	0.01	[–0.11, –0.02]

The changes are shown as trends ($km\ h^{-1}\ yr^{-1}$) and in percentage change over the period 1949–2016 in various regions and latitude belts. The regions include the North Atlantic, the western and eastern North Pacific and the northern Indian Ocean basins, and the Southern Hemisphere separated by 100° E. Other regions are separated by data over land and water, and by global latitude belts. Significance is shown by *P* values of the regressions and confidence intervals of the trends. Where identified by an asterisk, confidence intervals are based on effective degrees of freedom adjusted for serial correlation (see Methods). Significant trends, determined on the basis of the confidence interval, after correcting for serial correlation as needed, are shown in bold.

Extended Data Table 2 | Trends in tropical-cyclone translation speed and their statistics under the L^1 norm

	Trend ($km\ h^{-1}\ yr^{-1}$)	Change (%)	95% confidence interval of the trend
Global	**–0.03**	**–10**	[–0.04, –0.02]*
N. Hemisphere	**–0.03**	**–10**	[–0.05, –0.02]*
S. Hemisphere	**–0.03**	**–13**	[–0.05, –0.01]*
N. Atlantic	–0.03	–7	[–0.06, 0.007]
Western N. Pacific	**–0.06**	**–17**	[–0.07, –0.04]
Eastern N. Pacific	**–0.03**	**–13**	[–0.06, –0.007]
N. Indian	**+0.02**	**+13**	[0.002, 0.04]
S. Hemi. (<100°E)	–0.02	–8	[–0.04, 0.007]
S. Hemi. (≥100°E)	**–0.03**	**–10**	[–0.04, –0.006]
>35°N	–0.05	–9	[–0.13, 0.02]
25–35°N	**–0.04**	**–13**	[–0.07, –0.01]
15–25°N	**–0.02**	**–8**	[–0.03, –0.008]
0–15°N	–0.00	–1	[–0.02, 0.01]
0–30°S	**–0.03**	**–12**	[–0.04, –0.01]
> 30°S	+0.10	+25	[–0.003, 0.21]
Global (water)	**–0.03**	**–12**	[–0.04, –0.02]*
Global (land)	+0.01	+3	[–0.03, 0.05]*
N. Atlantic (land)	–0.04	–11	[–0.10, 0.03]
W. N. Pacific (land)	**–0.07**	**–19**	[–0.13, –0.02]*
E. N. Pacific (land)	–0.03	–11	[–0.21, 0.15]*
N. Indian (land)	+0.05	+22	[–0.001, 0.10]*
S. Hemi. (<100°E, land) Madagascar	–0.01	–3	[–0.06, 0.04]
S. Hemi. (≥100°E, land) Australia	**–0.06**	**–19**	[–0.11, –0.01]

Similar to Extended Data Table 1, but using an L^1 norm to calculate the trend statistics and test for robustness.